Supporting information for

Ru nanoclusters anchored on boron and nitrogen doped carbon for highly efficient hydrogen evolution reaction in alkaline seawater

Binbin Jiang[a], Zhen Wang[1a], Hui Zhao[a], Xie Wang[a], Xiaoxia Mao[a], Aijian Huang[b]*, Xuehua Zhou[a], Kui Yin[c]*, Kefa Sheng[a], Junwei Wang[a]*

a Anhui Key Laboratory of Photoelectric-Magnetic Functional Materials, Anhui Key Laboratory of Functional Coordination Compounds, School of Chemistry and Chemical Engineering, Anqing Normal University, Anqing 246011, China

b School of Electronics Science and Engineering, University of Electronic Science and Technology of China, Chengdu, 610054, China.

c Jiangsu Key Laboratory for Carbon-Based Functional Materials & Devices, Institute of Functional Nano & Soft Materials (FUNSOM), Soochow University, Suzhou, 215123, PR China

Experimental section

1.1 Materials

$RuCl_3 \cdot xH_2O$, dicyandiamide, boracic acid, soluble starch and hydrogen fluoride were purchased from Sinopharm Chemical Reagent Co. Ltd. The Nafion (5 wt %) was obtained from Sigma-Aldrich Co. The commercial Pt/C (20 wt% Pt loaded on the carbon black) catalysts were obtained from Alfa Aesar Co. Silica nanospheres (SiO_2, 12 nm) was purchased from Shanghai Macklin Biochemical Co., LtD. Other reagents were analytical reagent grade without further purification. Doubly distilled water was used throughout the experiments (Resistivity > 18.2 MΩ cm).

1.2 Synthesis of boron and nitrogen doped carbon, nitrogen doped carbon, boron doped carbon and carbon

Boron and nitrogen doped carbon (NBC) was obtained according to followed precodure: dicyandiamide, boracic acid, soluble starch and SiO_2 are added in 30 mL deionized water with continue stirring for 5 h. After stirring, the products was achieved by freeze-drying technique over 24 h. The achieved precursors was annealing at 500 °C for 3 h at Ar atmosphere with a heating rate of 2 °C/min. Subsequently, the temperature was increasd to 900 °C for 3 h with a heating rate of 2 °C/min. After cool naturally, the black powder was named as SiO_2@NBC. The obtained SiO_2@NBC was treated with NaOH to remove the SiO_2. Following this, the black powders were washed by water and dried by freeze-drying, respectively. The lastly, the preparation of NBC was heat treatment at 600 °C for 2 h under H_2/Ar (v/v, 5% H_2) with a heating rate of 2 °C/min. The nitrogen doped carbon (NC), boron doped carbon (BC) and carbon (C) were obtained based on same method.

1.3 Synthesis of Ru nanoparticle/boron and nitrogen doped carbon

Ru/NBC was annealed at 500 ^oC under Ar atmosphere for 2 h with a heating rate of 5 °C/min, the achieved composite was named as Ru nanoparticle/NBC (Ru/NBC).

1.4 Materials characterizations

The phase and crystallography of catalysts were characterized by X-ray powder diffraction (XRD, Rigaku Ulitma IV diffractometer) with Cu Kα radiation (λ = 0.15406 nm). Scanning electron microscopy (SEM) was carried out by using a Zeiss Supra 55. The transmission electron microscope (TEM), high angle annular dark field scanning transmission electron microscopy (HAADF-STEM) and elemental mapping by Energy-dispersive X-ray spectrometry (EDS) were employed to characterize the catalysts with a FEI Tecnai F20 transmission electron microscope (accelerating voltage is 200 kV). High resolution HAADF-STEM was executed on FEI titan themis 200 with spherical aberration corrector. The

chemical states of catalysts were studied using the X-ray photoelectron spectroscopy (XPS) measurement performed on Escalab 250Xi with Al Kα radiation (1486 eV) as a probe.

1.5 Details of computational calculations

All of the calculations were performed by means of spin polarized density functional theory (DFT) methods using the Vienna Ab initio Simulation Package (VASP).[S1] While the projector augmented wave (PAW) method was adopted to describe electron-ion interaction.[S2] The Perdew-Burke-Ernzerhof (PBE) exchange-correlation functional within a generalized gradient approximation (GGA) was employed, and a 520 eV cut off energy for the plane-wave basis set was used for the valence electrons. The self-consistent filed (SCF) calculations were performed with an energy and force convergence criterion of 10^{-5} eV and 0.02 eV $Å^{-1}$, respectively. And the intrinsic dipole correction was also considered in all DFT calculations. The Brillouin zone was sampled using the 2×2×1 Monkhorst-Pack sampling in structure optimization for periodically repeated metal slabs with maximum symmetry applied to reduce the number of k-points in the calculations. To avoid the interactions between two adjacent periodic images, the vacuum thickness was set to be 15 Å. The atomic structures were analyzed by using the VESTA code. [S3]

The integral adsorption energy for H atoms is defined by:

$$\Delta E_H = E(\text{surface} + H) - E(\text{surface}) - \frac{1}{2}E(H_2) \quad (1)$$

where the $E(\text{surface} + H)$ and $E(\text{surface})$ are the total energy of metal surface with H atoms adsorption and without, respectively. $E(H_2)$ is the total energy of hydrogen molecule in the gaseous phase. The Gibbs free energy of H atoms (ΔG_H) is an important parameter for the descriptor of HER activity:

$$\Delta G_H = \Delta E_H + \Delta ZPE - T\Delta S \quad (2)$$

where ZPE is the zero-point vibrational energy using the harmonic approximation, T is the kelvin temperature, and S is the entropy. According to thermodynamics, large positive values of ΔG_H indicate that the hydrogen atom is difficult to bind to the catalytic sites, whereas large negative values of ΔG_H indicate that molecular hydrogen is difficult to be released from the catalytic site.[S4] Therefore, tuning the ΔG_H approaching to zero is favorable for catalyst performance.

The kinetic energy barrier of the initial water dissociation step (ΔG_{H2O}) is applied as an activity descriptor for HER under alkaline condition, which can be calculated as follows:

$$\Delta G_{H2O} = G_{ts} - G_{ini} \quad (3)$$

where G_{ts} and G_{ini} are the free energy of the transient state and the initial state for water dissociation, respectively. The climbing image nudged elastic band (CI-NEB) method and dimer method implemented in VASP was used to determine the diffusion energy barrier and the minimum energy pathways.[S5, S6]

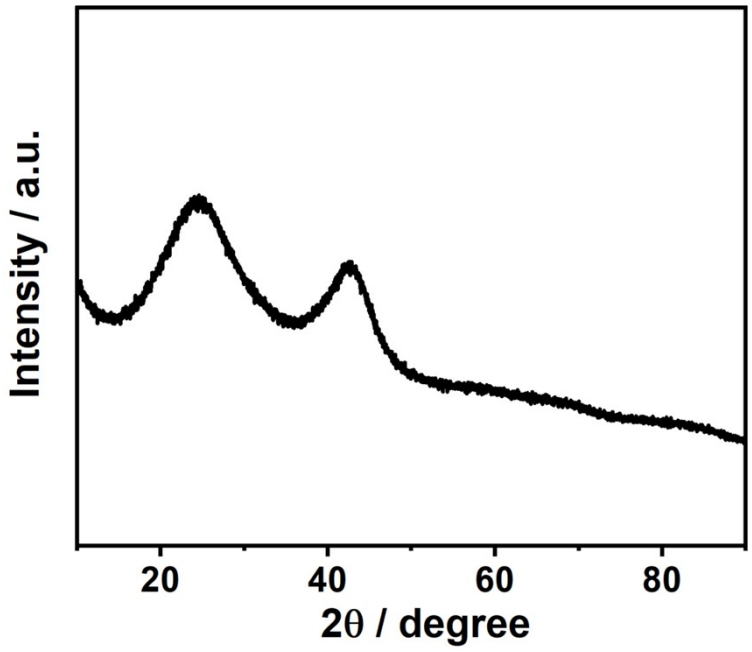

Fig. S1. The XRD patterns of Ru/NC.

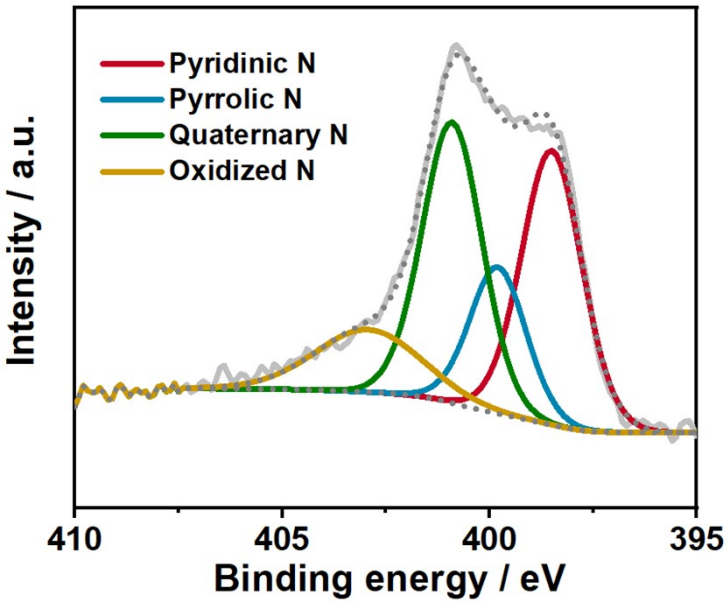

Fig. S2. The N 1s XPS spectra of Ru/C.

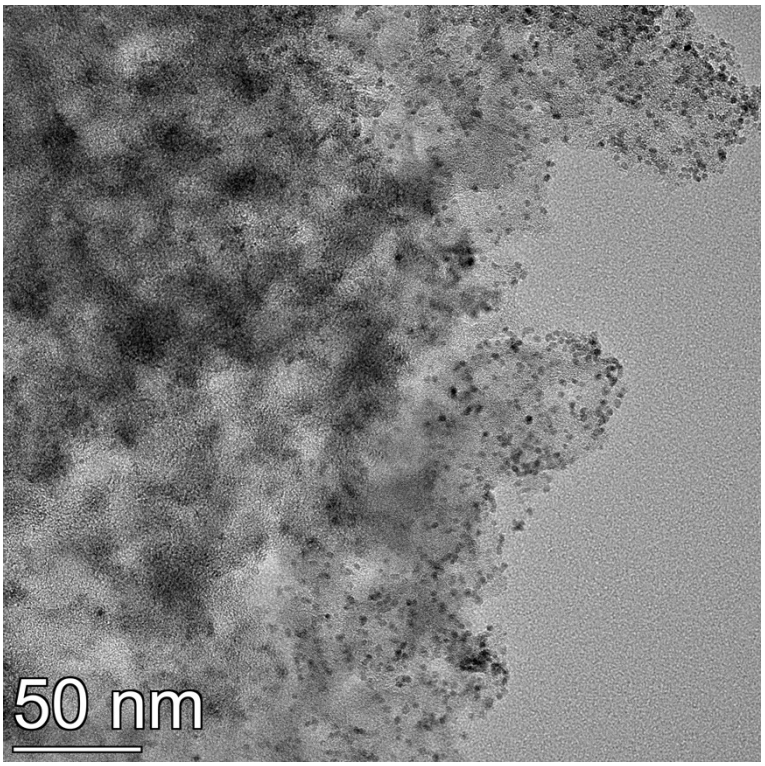

Fig. S3. The TEM image of Ru/NC.

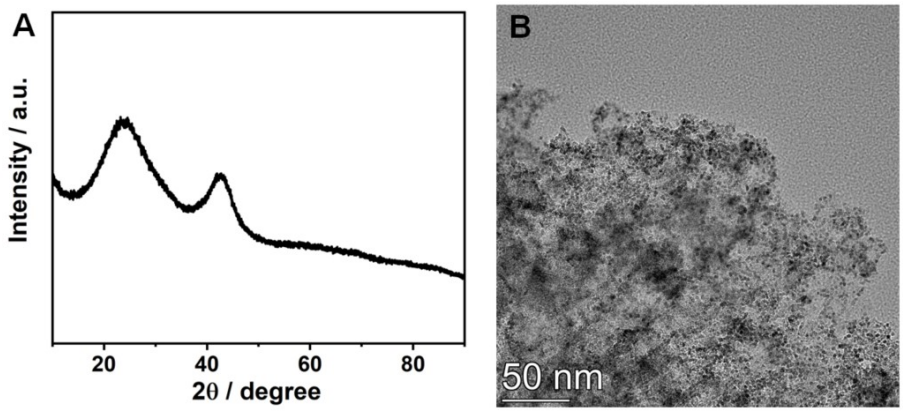

Fig. S4. (**A**) XRD pattern and (**B**) TEM image of Ru/BC.

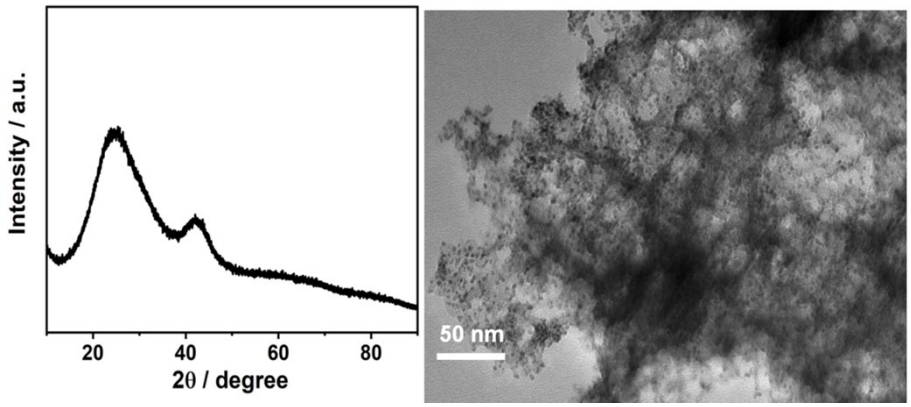

Fig. S5. (**A**) XRD pattern and (**B**) TEM image of Ru/C.

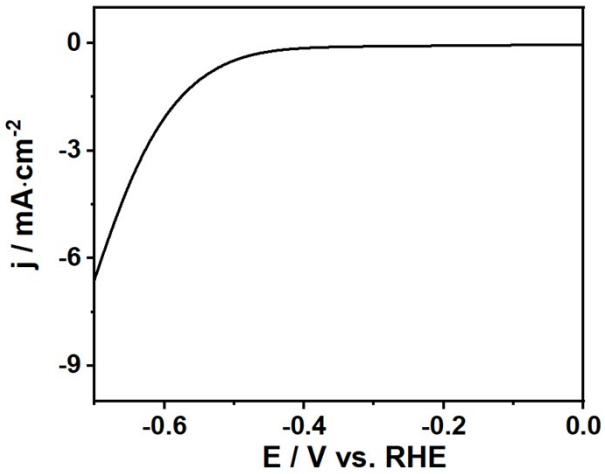

Fig. S6. The LSV curves of NBC in 1.0 M KOH.

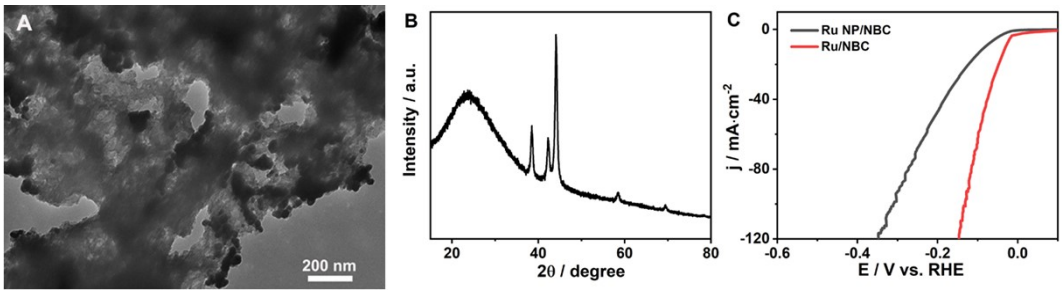

Fig. S7. (**A**) TEM image of Ru NP/NBC, (B) XRD pattern of Ru NP/NBC, and (**C**) LSV curve of Ru NP/NBC in 1.0 M KOH.

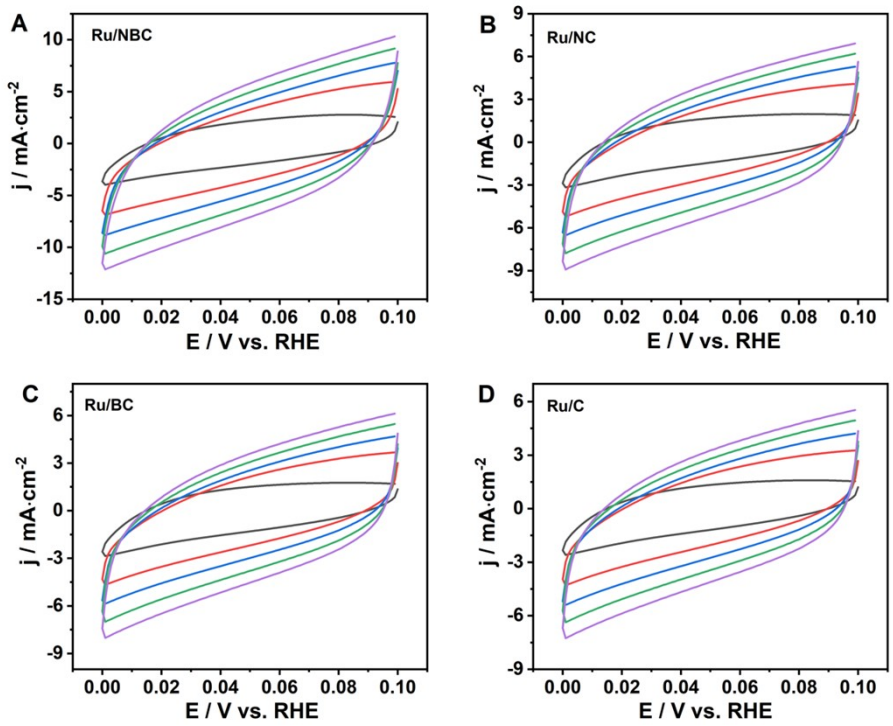

Fig. S8. The CV curves of (**A**) Ru/NBC, (**B**) Ru/NC, (**C**) Ru/BC and (**D**) Ru/C in 1.0 M KOH at scan rate of 20, 60, 100, 140 and 180 $mV \cdot s^{-1}$.

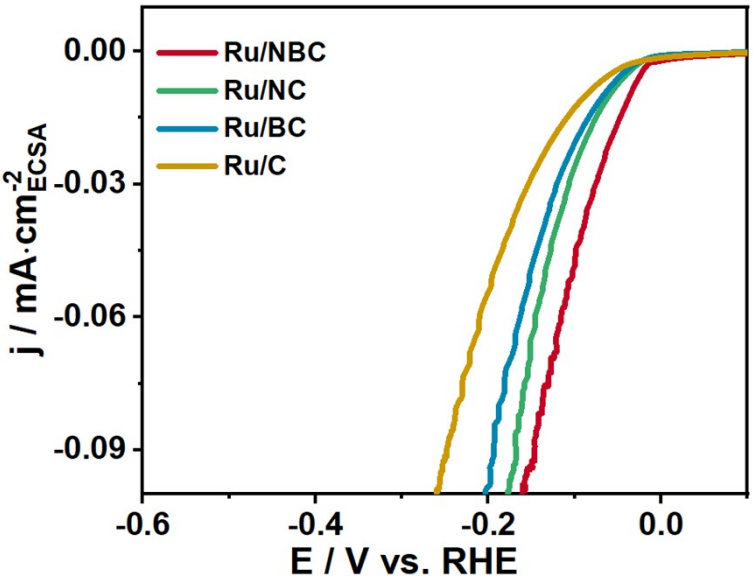

Fig. S9. Specific activity of as-prepared electrocatalysts.

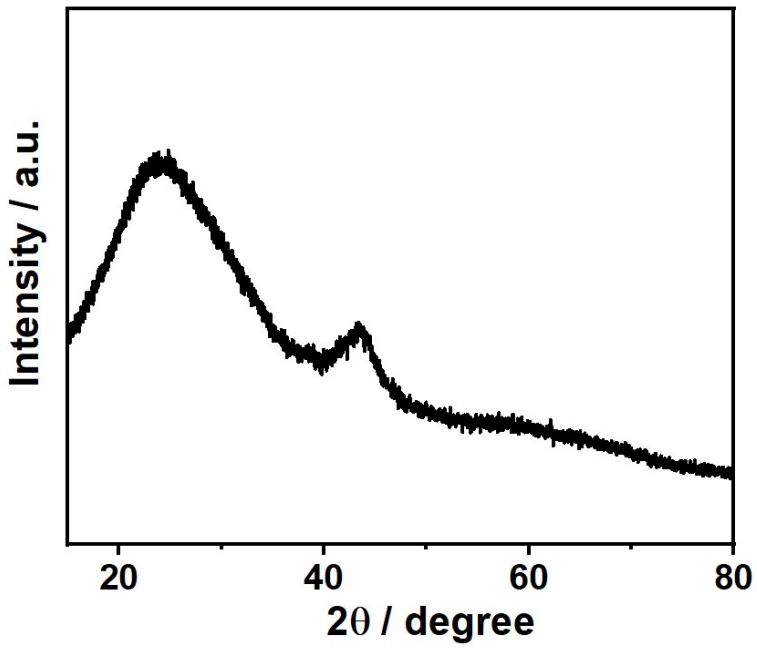

Fig. S10. XRD pattern of Ru/NBC after V-t test in 1.0 M KOH.

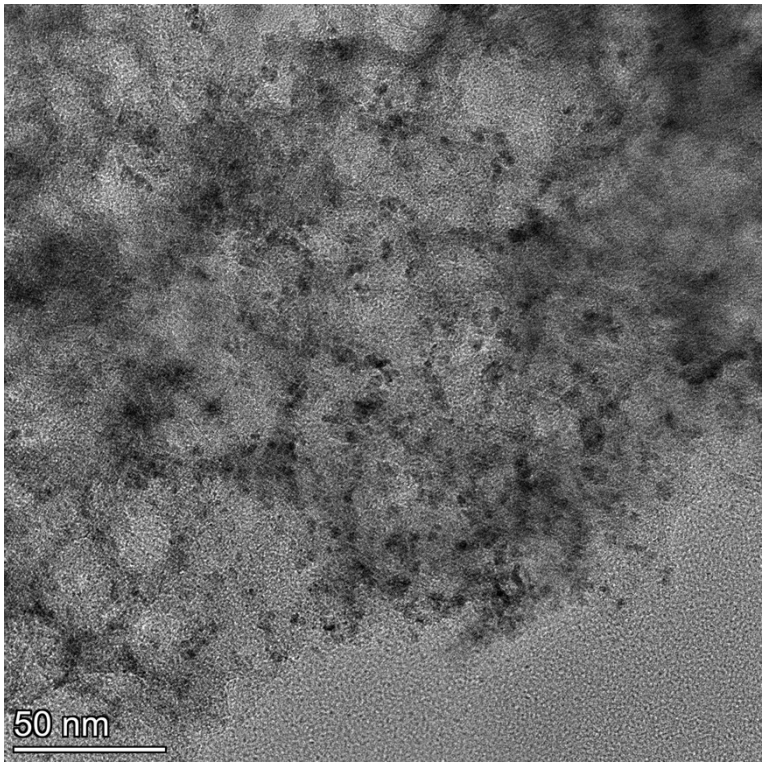

Fig. S11. TEM image of Ru/NBC after V-t test in 1.0 M KOH.

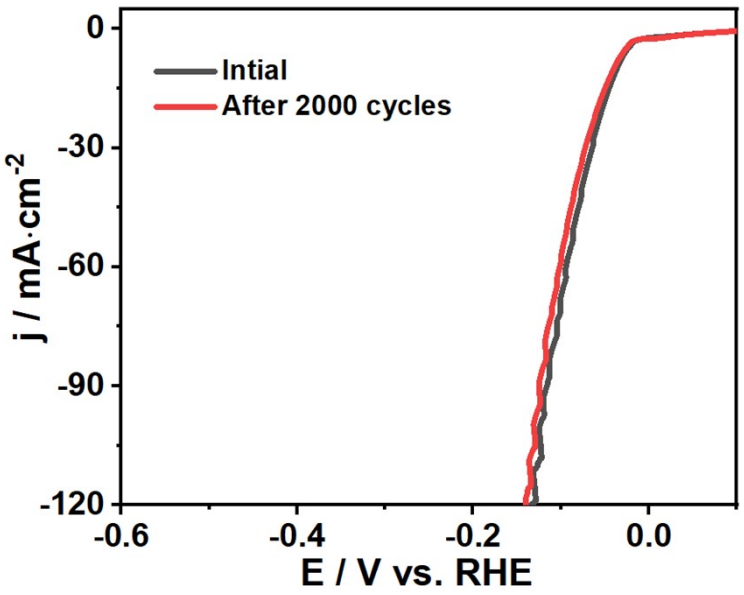

Fig. S12. LSV curves of Ru/NBC before and after CV test in 1.0 M KOH.

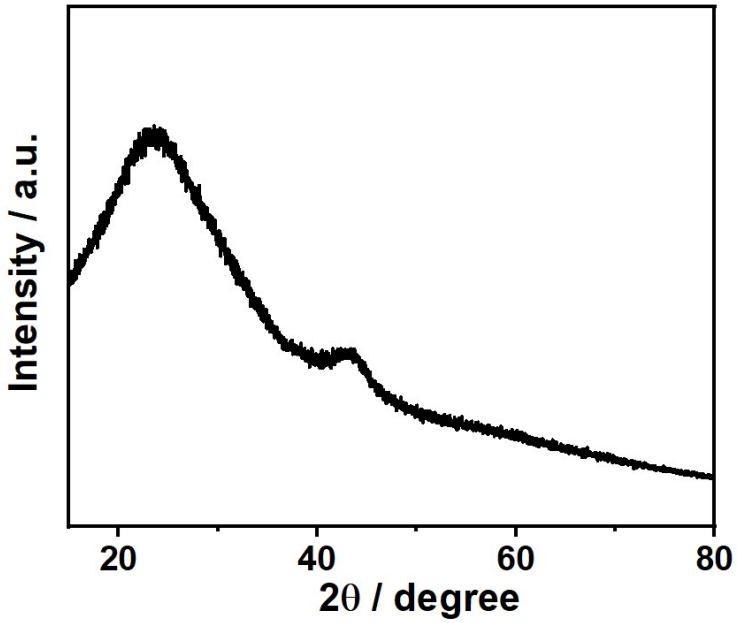

Fig. S13. XRD pattern of Ru/NBC after CV test in 1.0 M KOH.

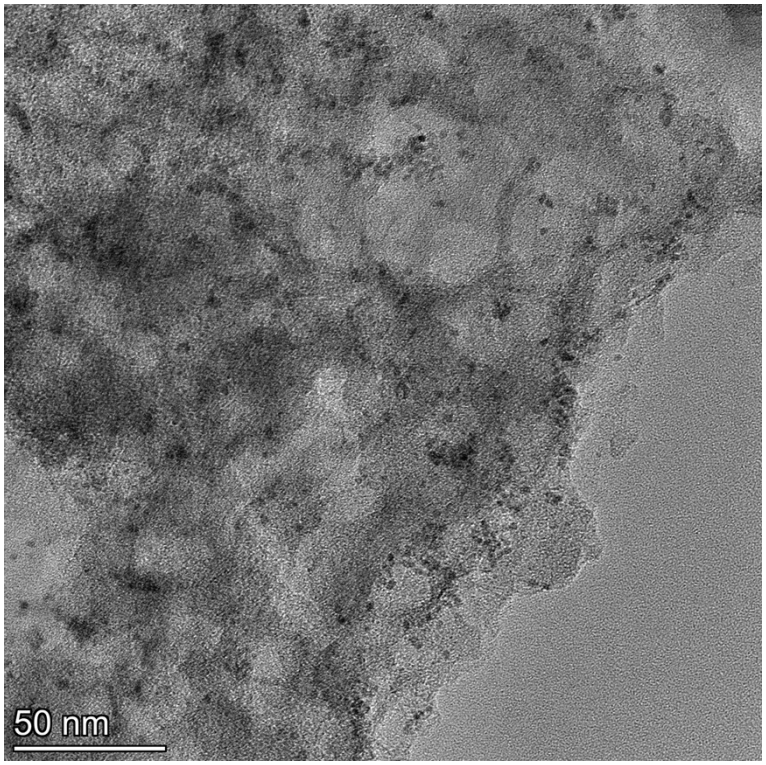

Fig. S14. TEM image of Ru/NBC after CV test in 1.0 M KOH.

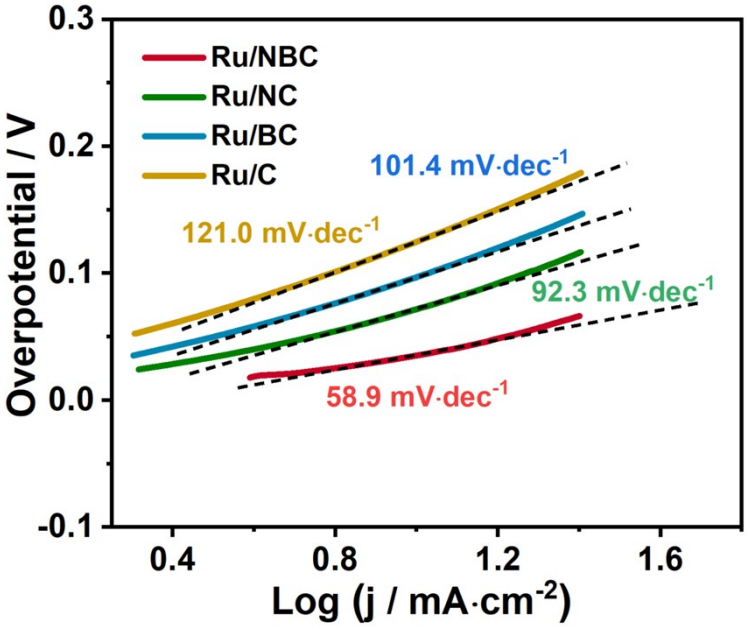

Fig. S15. The Tafel slope of as-prepared electrocatalysts in alkaline seawater.

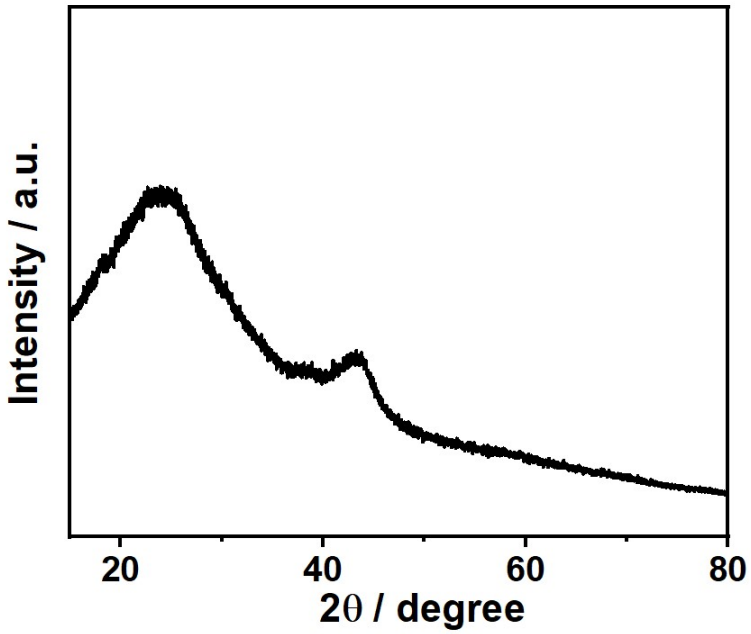

Fig. S16. XRD pattern of Ru/NBC after V-t test in 1.0 M KOH + seawater.

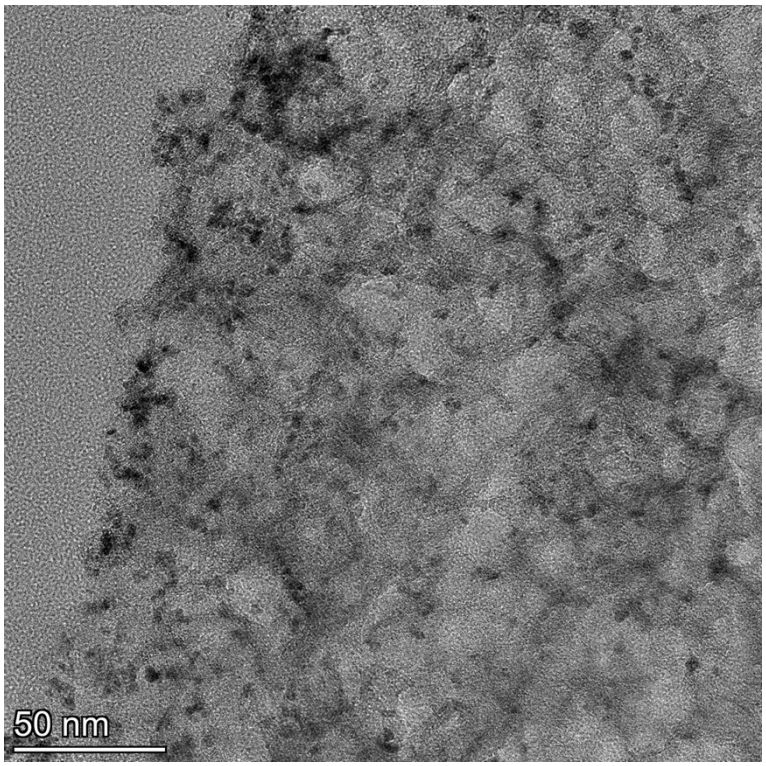

Fig. S17. TEM image of Ru/NBC after V-t test in 1.0 M KOH + seawater.

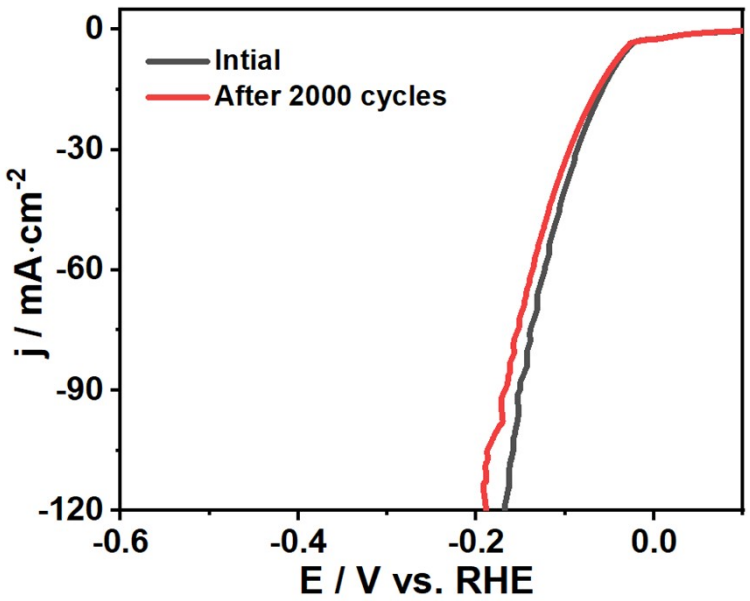

Fig. S18. LSV curves of Ru/NBC before and after CV test in 1.0 M KOH + seawater.

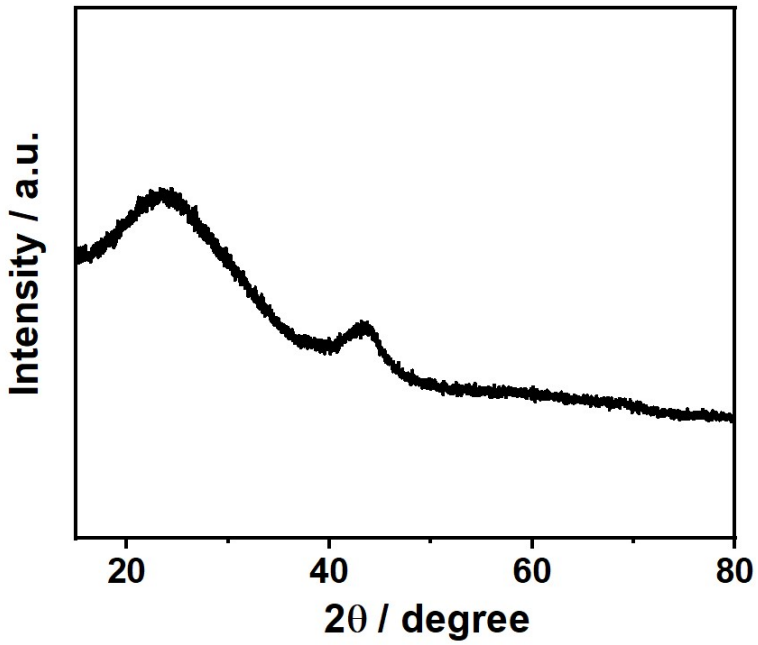

Fig. S19. XRD pattern of Ru/NBC after CV test in 1.0 M KOH + seawater.

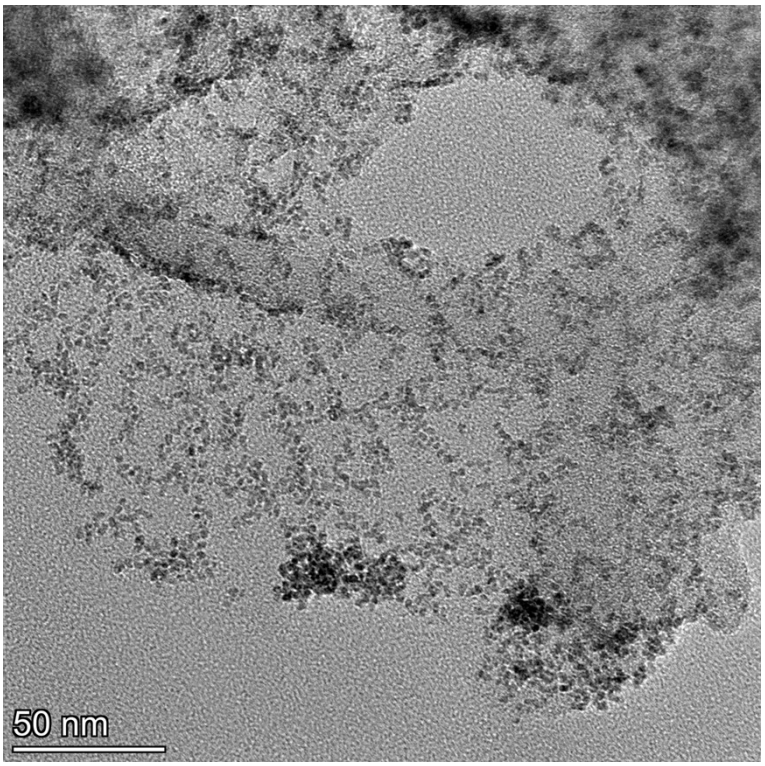

Fig. S20. TEM image of Ru/NBC after CV test in 1.0 M KOH + seawater.

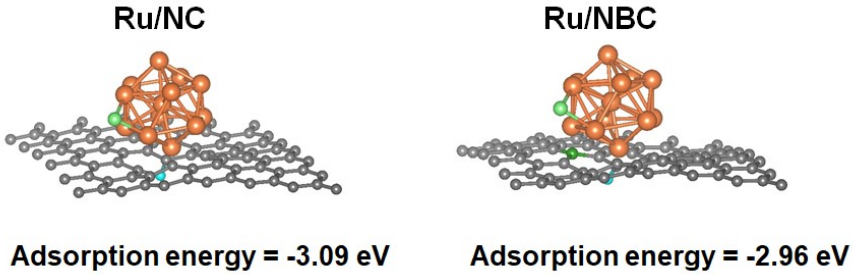

Fig. S21. The adsorption energy of Cl^- on Ru/NC and Ru/NBC surface.

Table S1. Comparison of HER activity among Ru based electrocatalysts with Ru/NBC in alkaline media.

Catalysts	**Overpotential at 10 mA·cm^{-2} (mV)**	**Tafel slope (mV·dec^{-1})**	**Reference**
Ru/NBC	**30**	**41.4**	**This work**
Ru NCs/BNG.	14	28.9	Nano Energy, 2020, 68, 104301
RuNP@RuN$_x$-OFC/NC	19	35.5	Appl. Catal. B Environ., 2022, 307, 121193.
RuCo@NC-600	36	39	J. Mater. Chem. A, 2020,8, 12810-12820
Ru/D-NPC	23	38	Appl. Catal. B Environ., 2022, 306, 121095
Ru@Ni-MOF	22	40	Angew. Chem. Int. Ed., 2021, 60, 22276-22282
Ru MNSs	24	22.3	Angew. Chem. Int. Ed., 2022, 61, e2021168.
NiRu$_{0.13}$-BDC	34	32	Nat. Commun., 2021, 12, 1369.
Ru$_{NP}$-Ru$_{SA}$@CFN-800	33	37.16	Adv. Funct. Mater., 2023, 33, 2213058
V$_O$-Ru/HfO$_2$-OP	39	29	Nat. Commun., 2022, 13, 1270.
Ru$_{1+NPs}$/N-C	39	27.6	ACS Appl. Mater. Interfaces, 2022, 14, 15250−15258
Ru SAs/N-Mo$_2$C NSs	43	38.67	Appl. Catal. B Environ., 2020, 277, 119236
Ru ND/C	43.4	49	Chem. Commun., 2018, 54, 4613-4616
Ru@1T-MoS$_2$-MXene	44	47	Adv. Funct. Mater., 2023, 2212514
Ru-NiCoP/NF	44	45.4	Appl. Catal. B Environ., 2020, 279, 119396.
Ru@Co/N-CNTs-2	48	43	ACS Sustainable Chem. Eng., 2020, 8, 24, 9136-9144.
Ru$_1$CoP/CDs-1000	51	73.7	Angew. Chem. Int. Ed., 2021, 60, 7234-7244
SA-Ru-MoS$_2$	76	21	Small Methods, 2019, 1900653
RuP$_2$@PC	78.9	36.7	J. Mater. Chem. A, 2021, 9, 12276-12282.
PtRu/CC-P	44	45.1	Nanoscale, 2022, 14, 15942–15949
Cu$_{2-x}$S@Ru NPs	82	48	Small, 2017, 13, 1700052

Table S2. Comparison of HER activity among Ru based electrocatalysts with Ru/NBC in alkaline seawater.

Catalysts	**Overpotential at 10 mA·cm^{-2} (mV)**	**Tafel slope (mV·dec^{-1})**	**Reference**
Ru/NBC	**35**	**58.9**	**This work**
Ru_{1+NPs}/N−C	58	-	ACS Appl. Mater. Interfaces, 2022, 14, 15250−15258
Ni-SA/NC	139	61	Adv. Mater., 2021, 33, 2003846
1D-Cu@Co-CoO/Rh	137.7	124.8	Small, 2021, 17, 2103826
cRu-Ni_3N/NF	36	-	Energy Environ. Mater., 2023, 6, e12318
l-Rh metallene	38	39.0	Appl. Catal. B Environ., 2022, 310, 121338
c-Rh metallene	49	45.3	Appl. Catal. B Environ., 2022, 310, 121338
Ru_2P@Ru/CNT	29	-	Chin. J. Catal., 2022, 43, 1148-1155.
Ni-MoN	29	-	Adv. Mater., 2022, 34, 2201774
Ni_3N/W_5N_4	36	43	Appl. Catal. B Environ., 2022, 307, 121198.
NiFeP-NS	59	97.0	Appl. Catal. B Environ., 2022, 302, 120862
$Ru_{1,n}$-$ZnFe_2O_x$-C	15.9	-	Small, 2022, 18, 2204155

References

S1 G. Kresse, *Phys. Rev. B*, 1996, **54**, 11169.

S2 G. K. J. Furthmu¨Ller, *Phys. Rev. B*, 1999, **54**, 11169.

S3 K. Momma, F. Izumi, *J. Appl. Crystallography*, 2008, 41, 653.

S4 J. K. Nørskov, T. Bligaard, A. Logadottir, J. R. Kitchin, J. G. Chen, S. Pandelov, U. Stimming, *J. Electrochem. Soc.*, 2005, **152**, J23

S5 B. P. U. Graeme Henkelman, J. Hannes, *J. Chem. Phys.*, 2000, **113**, 9901.

S6 A. H. J. Graeme Henkelman, *J. Chem. Phys.*, 1999, **111**, 7010.